Original Research

Assessment of Regional Lung Function Impairment in Airway Obstruction and Pulmonary Embolic Dogs With Combined Noncontrast Electrocardiogram-Gated Perfusion and Gadolinium Diethylenetriaminepentaacetic Acid Aerosol Magnetic Resonance Images

Nobuhiko Ogasawara, MD, Kazuyoshi Suga, MD,* Yasuhiko Kawakami, MD, Tomio Yamashita, MD, Mohammed Zaki, MD, and Naofumi Matsunaga, MD

Purpose: To define regional function impairment in airway obstruction (AO) and pulmonary embolic (PE) dogs with a combination study of noncontrast electrocardiogram (ECG)-gated perfusion and gadolinium diethylenetriaminepentaacetic acid (Gd-DTPA) aerosol magnetic resonance (MR) images.

Methods: After acquisition of multiphase fast-spin-echo (FSE) MR images during cardiac cycles in 14 AO dogs and 19 PE dogs, ECG-gated perfusion-weighted (PW) images were obtained by subtraction between two-phase images of the minimum lung signal intensity (SI) during systole and maximum SI during diastole. Each dog subsequently inhaled Gd-DTPA aerosol for 20 minutes, and subtracted Gd-DTPA aerosol images were obtained from precontrast and maximally enhanced images. ECG-gated PW images were compared with intravenous Gd-DTPA-enhanced pulmonary arterial perfusion phase (PAPP) images.

Results: ECG-gated PW images were consistent with Gd-DTPA-enhanced PAPP images in all dogs, with significant correlations in the affected-to-unaffected lung perfusion ratios ($P < 0.005$). Gd-DTPA aerosol images showed sufficient and uniform enhancement in the unaffected lungs. In all the AO areas, these combined images showed the matched perfusion and aerosol deposition defects. These images showed perfusion defects without aerosol deposition defects in the relatively small embolized areas, but showed the matched defects in the widely embolized areas probably due to hypoxic bronchial constriction.

Conclusion: The combination MR studies may be acceptable for noninvasively defining regionally impaired lung function in AO and PE.

Key Words: lung ventilation; lung perfusion; magnetic resonance (MR) imaging; gadolinium; aerosol; electrocardiogram (ECG) gating; experimental study
J. Magn. Reson. Imaging 2004;20:46–55.

ALTHOUGH A RADIONUCLIDE SCINTIGRAPHY is widely used in the evaluation of regionally impaired ventilation and perfusion in various lung diseases, this technique has the inherent disadvantages of the need to use radioactive substances and the poor spatial/temporal resolution images. To resolve these problems, several magnetic resonance imaging (MRI) techniques have been proposed (1–12). Gadolinium diethylenetriaminepentaacetic acid (Gd-DTPA) aerosol and electrocardiogram (ECG)-gated short-echo-spacing half-Fourier fast-spin-echo (FSE) perfusion MR images are also expected to be widely available, noninvasive, low-cost approaches (13–22). The ECG-gated FSE MR technique enables the image acquisition of the pulsatile lung signal intensity (SI) changes during a cardiac cycle without use of any contrast materials, and a subtraction process between the systolic and diastolic phase images can be expected to provide lung perfusion images (18–21). The aerosol MR technique provides efficient Gd-DTPA aerosol deposition in the lung using an open-circuit aerosol delivery system (13,22). A combination study of these noncontrast ECG-gated perfusion and Gd-DTPA aerosol MR images may have potential utility for simultaneous assessment of regional perfusion and ventilation in the same subject. This is the preliminary experimental study to evaluate the ability of these combination MR images in the definition of regionally impaired lung function in fundamental dog models of

Department of Radiology, Yamaguchi University School of Medicine, Ube, Yamaguchi, Japan.
Contract grant sponsor: Grants for Scientific Research from the Japanese Ministry of Education, Science, Sports & Culture; Contract grant numbers: 11670891, 14570860.
*Address reprint requests to: K.S., Department of Radiology, Yamaguchi University School of Medicine, 1-1-1 Minamikogushi, Ube, Yamaguchi 755-8505, Japan. E-mail: sugar@po.cc.yamaguchi-u.ac.jp
Received September 3, 2003; Accepted February 5, 2004.
DOI 10.1002/jmri.20087
Published online in Wiley InterScience (www.interscience.wiley.com).

acute airway obstruction (AO) and pulmonary embolism.

MATERIALS AND METHODS

Animal Preparations

In accordance with the guide for the care and use of laboratory animals (23), and with approval by the Animal Care and Research Use Committee, a total of 33 adult beagle dogs (10.5 ± 1.2 kg) were intubated with a 7-mm endotracheal tube after receiving sodium pentobarbital (25 mg/kg) and ketamine hydrochloride (20 mg/kg). Small supplementary doses of sodium pentobarbital (total dose ranged from 3.1–6.8 mg/kg) were intermittently administered during the course of the experiment as needed to maintain the steady heart rate and respiration rate of the dogs during experiments.

In 14 of these anesthetized dogs, the secondary bronchus in the unilateral lower lung was selectively occluded using a 5-French balloon catheter under x-ray fluoroscopic guidance, by inflating the balloon with an injection of 0.3–1.5 mL physiologic saline. After confirming adequate placement of the balloon catheter in the selected bronchus, the balloon was deflated and the catheter was fixed on the animal body. These dogs underwent an ECG-gated perfusion MR study before inflating the balloon to evaluate the perfusion appearance in the normal lungs. Thereafter, at 50 minutes after inflating the balloon with injection of the same dose of physiologic saline, these dogs again underwent an ECG-gated perfusion MR study, immediately followed by the Gd-DTPA aerosol and intravenous Gd-DTPA-enhanced dynamic MR studies, as described below. Soon after accomplishment of these MR studies, each dog underwent x-ray fluoroscopy without withdrawing the inflated balloon catheter from the obstructed bronchus to confirm an adequate placement of the intrabronchial balloon and to evaluate the volume change of the obstructed lungs.

In the remaining 19 anesthetized dogs, under x-ray fluoroscopic guidance, the unilateral pulmonary arteries supplying blood flow to the lower lungs were selectively embolized by injection of enbucrilate (Histoacryl, B. Braun Surgical GmbH, Melsungen, Germany) via a 4-French pulmonary angiographic catheter (Cook, Bloomington, IN). The catheter was inserted from the jugular vein of the animals using the Seldinger technique. Enbucrilate released from a catheter produces a coagulant soon after contact with blood, resulting in variable-size pulmonary emboli (12,13). The embolization was confirmed by pulmonary arteriography with a rapid bolus injection of 12–18 mL of iopamidol (Iopamiron-370, Nippon Shering, Osaka, Japan) via the 5-French balloon catheter replaced at the pulmonary artery trunk. Ten minutes after embolization, each dog underwent the ECG-gated perfusion MR study, immediately followed by the Gd-DTPA aerosol and intravenous Gd-DTPA-enhanced dynamic MR studies.

ECG-Gated FSE Perfusion MR Images

All the MR experiments were performed using a 1.5-Tesla MR system (VISART/EX, Toshiba Medical, Tokyo, Japan) with a maximum gradient strength of 40 mT/m and a slew rate of 150 mT/m/msec. Each dog was placed in the supine position on a quadrature radio frequency (RF) knee coil, and two copper electrodes were placed in the anterior chest wall to obtain an ECG gating. Mid-coronal localizer fast-gradient T1-weighted images of the lung were initially acquired. In the AO dogs, mid-coronal localizer FSE T2-weighted images were also obtained to confirm adequate placement of the balloon after inflating the balloon of the intratracheal catheter as in x-ray fluoroscopy. Based on these localizer images, a preparation scan of ECG-gated multiphase FSE images was obtained at the selected single-slice level of the affected lower lung to determine the trigger times after the R-wave for obtaining the diastolic image showing the maximum lung SI and the systolic image showing the minimum lung SI in each dog. In this preparation scan, consecutive images were acquired with an interval time of 20 msec between an R-wave and the next R-wave, with eight shots and two excitations (Fig. 1). The sequence parameters were as follows: effective repetition time (TReff)/effective echo time (TEeff)/echo train spacing = two R-R-wave intervals/80 msec/4 msec, matrix = 224 × 256, field of view (FOV) = 30 × 30 cm, and slice thickness = 20 mm. A short echo train spacing of 4 msec and an effective TEeff of 80 msec were used because they expected to show high SI in relatively slow flow during cardiac diastole and low SI in high blood flow during systole (13–16). The relatively greater slice thickness of 20 mm was applied in this preliminary study to obtain high SI in the lung. The data collection was applied as half-Fourier FSE, early echoes were placed near the zeroth encode, later echoes were filled in at higher frequencies in k-space, and the total echo train length was determined using a contrast echo train length, the data points filling the half-Fourier part of the k-space, and a half phase encode matrix. In each of eight shots, 34 lines of echo train length, including the upper half of k-space of 20 lines and the lower half of k-space of 14 lines, were acquired. One shot acquisition time was 136 msec for this echo train length of 34 lines. In a total of eight shots

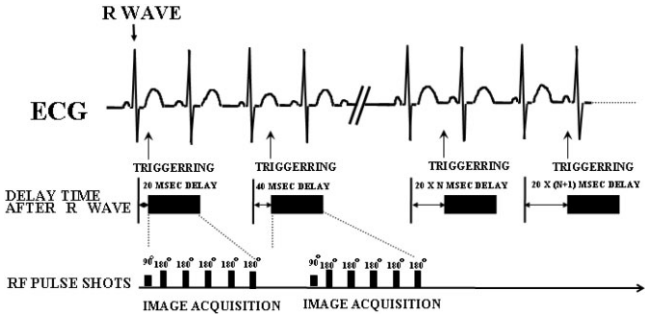

Figure 1. The multiphase short-echo-spacing ECG-gated FSE MR sequence for a preparation scan. The consecutive multiphase images were acquired using eight RF pulse shots, with an interval time of 20 msec between the R-R-waves on the ECG. From this preparation scan, the trigger times after the R-wave for obtaining the diastolic image showing the maximum lung SI and the systolic image showing the minimum SI are determined.

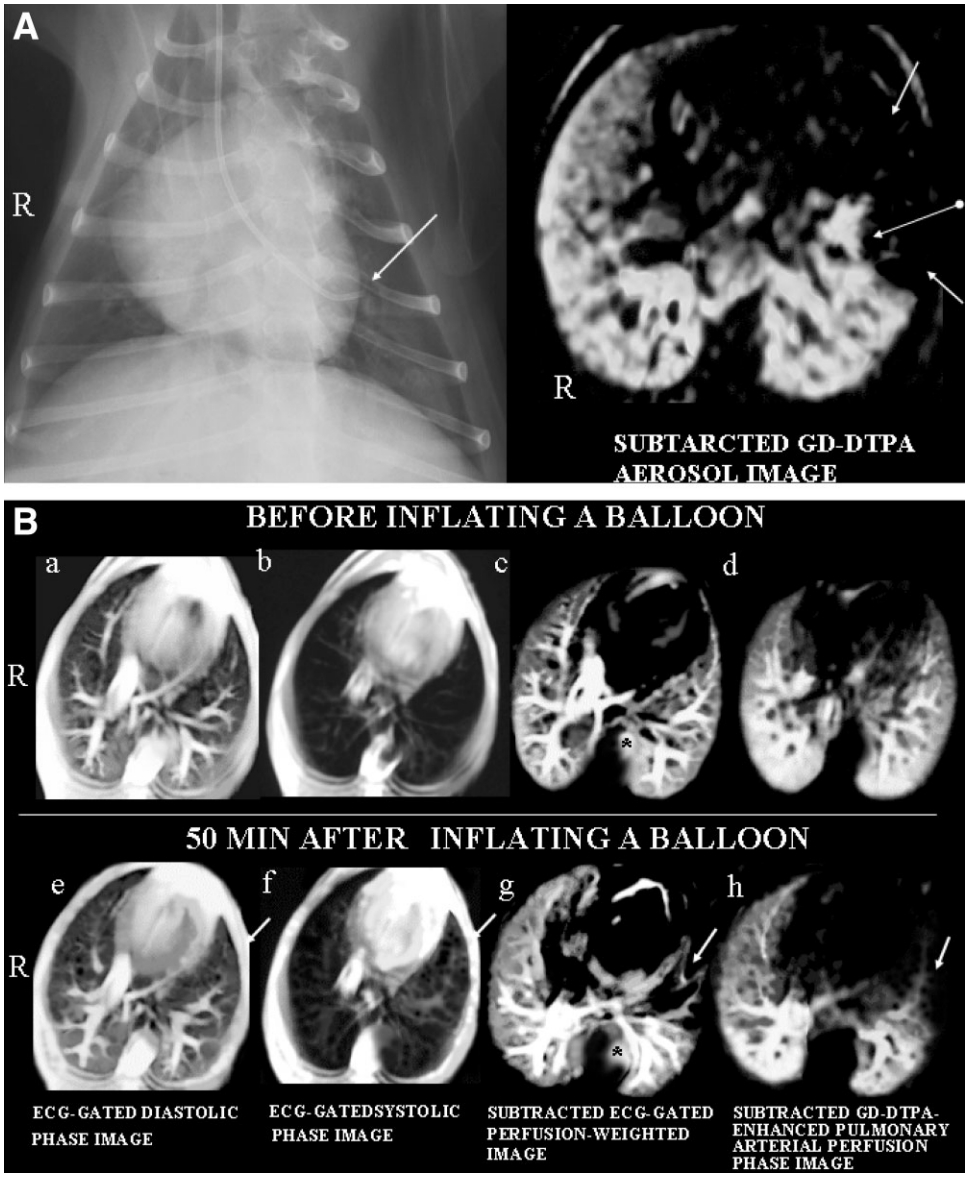

Figure 2. MR studies in an AO dog. **A:** A chest radiograph (left) shows the balloon catheter placed within the bronchus of the left lower lung (left, arrow). The subtracted Gd-DTPA aerosol MR image shows the aerosol deposition defect in the left lung area distal to bronchial occlusion (right, arrowS), with a focal aerosol hyperdeposition within the proximal lumens of the occluded bronchi (●→). **B:** Before inflating the balloon (top), the ECG-gated diastolic phase image (TReff/TEeff = 824/80 msec) (a) shows an apparently higher SI of the lung parenchyma and pulmonary arteries than does the systolic phase image (b). The subtracted ECG-gated PW image (c) shows a fairly uniform perfusion, similar to the subtracted intravenous Gd-DTPA-enhanced PAPP image (d). However, at 50 minutes after inflating the balloon (bottom), the ECG-gated diastolic and systolic phase images (e and f) show a persistently high SI in the affected area (arrows), although the normally appearing SI loss during systole is seen in the unaffected lung area. The subtracted ECG-gated PW image (g) shows the perfusion defect in the affected area (arrow), which is nearly consistent with the subtracted intravenous Gd-DTPA-enhanced PAPP image (h, arrow). The location and extent of the perfusion defect nearly match those on the Gd-DTPA aerosol deposition defect (A). * = The round structure is the descending thoracic aorta (c, g). **C:** Before inflating the balloon, the time-SI curves of the lung parenchyma (top) and pulmonary artery (bottom) on the ECG-gated preparation scan show the synchronized signal changes, with SI increases during diastole and decreases during systole. Tmin = time delay after the R-wave showing the minimum SI, Tmax = time delay after the R-wave showing the maximum SI, ΔSIECG = the difference between the maximum and minimum SI. **D:** At 50 minutes after inflating the balloon, the curves of the lung parenchyma (top) and pulmonary artery (bottom) become almost flattened throughout a cardiac cycle.

data collection, a total echo train length of 272 lines was acquired. Therefore, 48 lines were removed for the k-space from the first lines in the 160 lines in the upper half of the k-space.

Therefore, the first six lines in the eight shots were removed. In the AO dogs, this preparation scan was performed twice, i.e., before and immediately after bronchial occlusion. Using the two determined delay

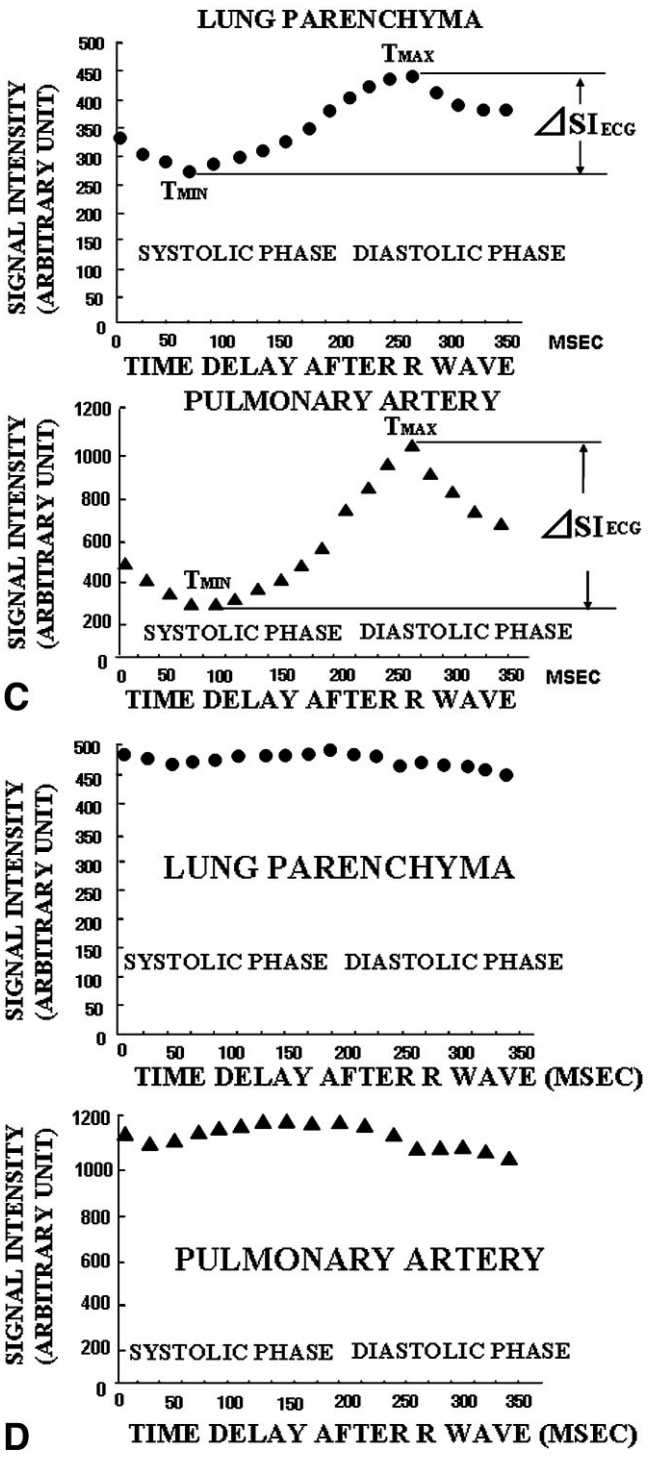

Figure 2 (Continued)

times after the R-wave at the systolic and diastolic phases in each dog, a two-phase scan of ECG-gated FSE MR images was then obtained using 12 NEX to increase the signal-to-noise ratio (SNR). The heart rate of the 33 dogs varied from 97–191 beats/minute, and TReff ranged from 584–1012 msec (mean = 867 msec ± 72). ECG-gated image acquisition was completed within five minutes in all these dogs. A diastolic phase image of the ECG-gated two-phase images was then subtracted from a systolic phase image, yielding a noncontrast perfusion-weighted (PW) MR image.

Gd-DTPA Aerosol MR Images

A Gd-DTPA aerosol study was performed, as described previously (13,17). Immediately after an ECG-gated MR study, five consecutive precontrast images with a slice thickness of 4 mm were obtained using a three-dimensional (3D) fast-spoiled-gradient-recalled acquisition in the steady-state technique, with interval times of one minute at the same transaxial planes as in the ECG-gated study, also as described previously (13,17). Thereafter, the long tube of the aerosol delivery system was connected to the intubated tube of the dogs, aerosol inhalation was started, and 20 consecutive postcontrast MR images during Gd-DTPA aerosol inhalation were obtained with a 1-minute interval for 20 minutes. The maximally enhanced expiratory phase image was subtracted by the same lung-level precontrast image at the same expiratory phase. This subtraction was performed using two or three candidates of the precontrast expiratory phase image by referring to the time-course of lung SI changes, and the most adequately subtracted image with the minimum misregistration was applied.

Intravenous Gd-DTPA-Enhanced Dynamic MR Study

Following the Gd-DTPA aerosol study, each dog underwent a Gd-DTPA-enhanced dynamic perfusion MR study with a three-second intravenous bolus injection of a 0.1 mmol/kg dose of Gd-DTPA (Magnevist, Nippon Shering KK, Osaka, Japan), using a power injector. The dynamic images were acquired using a 3D fast-gradient-echo sequence, and the sequence parameters were as follows: TR/TE = 2.6/0.9 msec, flip angle = 30°, slab thickness = 80 mm, slice thickness = 8 mm, matrix size = 96 × 256, rectangular FOV = 270 × 360 mm, acquisition time = 2.8 seconds/scan. The center of the slab was set at the same lower lung level as in the ECG-gated MR study. A total acquisition time of 35 seconds produced a series of 12 or 13 transaxial images, and a series of 2 precontrast and 7 or 8 postcontrast images were obtained in each lung section. By referring to the time-course of lung SI changes, the pulmonary arterial perfusion phase (PAPP) image with the highest lung SI increase was subtracted from the second precontrast image at each lung level, which yielded a Gd-DTPA-enhanced PAPP image.

Image Interpretation and MR Signal Analysis

The subtracted noncontrast ECG-gated PW and Gd-DTPA aerosol MR images were viewed on a workstation (VISART/EX, Toshiba Medical, Shibaura, Japan) by two chest MR specialists (Y.K. and T.Y.) blinded to the information about the affected lung regions. The matching or mismatching of the perfusion and Gd-DTPA aerosol defects on these images and the consistency of the perfusion appearance between the noncontrast ECG-gated PW and intravenous Gd-DTPA-enhanced PAPP images were interpreted. The final

image interpretation was recorded after consensus was established.

To evaluate the normal SI changes of various structures on the ECG-gated preparation scans before inflating the intrabronchial balloon in the 14 AO dogs, the SI of the lung parenchyma, the pulmonary arteries/veins, the descending aorta, and the inferior vena cava were analyzed using a manually defined region of interest (ROI). Lung parenchymal SI was measured using the ROIs placed along the peripheral portions covering the ventral and dorsal lungs, but to minimize any contribution from large vessels and from the noticeable artifacts caused by fast cardiac motion. The time-course of SI changes was obtained for each ROI, and the percentage of the delay time after the trigger R-wave showing the minimum and maximum SIs against the R-wave interval time (%Tmin and %Tmax), and the difference between the maximum and minimum SIs (ΔSIECG = (the maximum SI–background noise SI)–(the minimum SI–background noise SI)) were estimated. The background noise was measured with a large ROI that encompassed the entire image background lateral to each animal. In the two dog models, the lung parenchymal ΔSIECG was measured for each ROI in the affected lung areas and in the contralateral unaffected areas.

In the Gd-DTPA aerosol study, ROI analysis was also performed in the peripheral portions of the affected and unaffected lung areas. The relative lung SI increase against the precontrast lung SI (%ΔSIaerosol) was estimated, and the mean values at each time point after aerosol inhalation in regional lungs were plotted on the time-course curves. The precontrast lung SI was determined by averaging the measurements of the five precontrast images. The maximum %ΔSIaerosol in each lung region was then determined by averaging the lung SI increases on the last three postcontrast images, since the maximum enhancement was always seen on these images.

In the intravenous Gd-DTPA-enhanced dynamic perfusion study, the mean lung SI was estimated in regional lungs, using the same ROIs as those used for the ECG-gated MR images, and the relative lung SI increase against the precontrast lung SI (%ΔSIGd-DTPA) at each time point was estimated using the following formula: ((postcontrast SI–precontrast SI)/precontrast SI) × 100%.

All the ROIs were placed independently by the two interpreters (K.S. and N.O.), and the data were taken as an average of the two measurements. The areas of the ROIs in the lung parenchyma ranged from 2.1–5.8 cm^2.

Statistical Analysis

Values were expressed as means with standard deviations (SDs). Significances in the differences of the lung SI between the diastolic and systolic phases and between the dorsal and ventral lungs in the normal lungs, those of the affected-to-unaffected lung ΔSIECG and %ΔSIGd-DTPA ratios, and those of the mean maximum %ΔSIaerosol between the embolized and nonembolized lung areas were evaluated by a paired Student's *t*-test. Significances in the differences of the mean ΔSIECG, %Tmin, and %Tmax between the large vessels and lung parenchyma were evaluated by an unpaired Student's *t*-test. Significant levels were accepted as *P* values of less than 0.05. A linear regression analysis was also performed to evaluate the correlation between the affected-to-unaffected ΔSIECG and %ΔSIGd-DTPA ratios, where a *P* value less than 0.05 was considered significant for each correlation coefficient (r).

RESULTS

Normal Dogs

ECG-gated FSE preparation scans before inflating the balloon in the 14 AO dogs showed apparent SI loss of the lung parenchyma during systole (Fig. 2). The time-course of the lung SI changes was synchronized with that of the pulmonary artery, although it was not synchronized with that of the other large vessels (Table 1). Both the ventral and dorsal lung ROIs in the diastolic phase had significantly higher SIs than those in the systolic phase (Table 2). The ΔSIECG was significantly greater in the dorsal lung than in the ventral lung areas, but without significant differences between the same gravitational lung portions. The subtracted ECG-gated PW images showed fairly uniform lung SIs, but with gravity-dependent gradient, with only minimal respiratory motion artifacts and vascular ghosting. The pulmonary arteries, at least to the subsegment levels, were clearly visualized, while the pulmonary veins appeared as lower SI structures.

AO Dogs

At 50 minutes after inflating the balloon, the affected lungs in the lower lung sections showed persistently high SI throughout a cardiac cycle on these preparation scans, although the normally appearing SI loss during systole was seen in the unaffected lungs (Fig. 2). There was a significant difference in the ΔSIECGs between the affected and unaffected lung areas (52.7 ± 27.4 vs. 178.7 ± 54.2; $P < 0.0001$). The subtracted ECG-gated PW images showed apparent perfusion defects in the airway-occluded lung areas in all these dogs, in consensus of two observers (Fig. 2). On the subtracted intravenous Gd-DTPA-enhanced PAPP images, the affected lung areas were less enhanced than the unaffected areas, with significantly lower %ΔSIGd-DTPA (133.3% ± 67.3 vs. 615.1% ± 148.8; $P < 0.0001$). The location and extent of these unenhanced areas were consistent with those on the subtracted noncontrast ECG-gated PW images (Fig. 2). However, after the PAPP images, some enhancement of the affected areas was seen, probably due to the anastomotic/collateral perfusion. There was a significant linear correlation between the affected-to-unaffected lung %ΔSIGd-DTPA and ΔSIECG ratios ($r = 0.720$, $P < 0.005$), although the mean ΔSIECG ratio was significantly greater than the mean %ΔSIGd-DTPA ratio (0.30 ± 0.14 vs. 0.21 ± 0.08; $P < 0.01$) (Fig. 3A).

In a Gd-DTPA aerosol study, the unaffected lung areas were gradually and uniformly enhanced with the maximum %ΔSIaerosol of 217.8 ± 62.4%, although no noticeable aerosol deposition was seen in the affected lung areas. Aerosol hyperdeposition, however, was seen

Table 1
ECG-Gated Perfusion MR Parameters in Normal Dog Lungs

Locations	%Tmin	%Tmax	Δ SI_{ECG}
Lung parenchyma (N = 28)	16.6 ± 1.9	53.6 ± 3.3	174.3 ± 50.4
Pulmonary artery (N = 28)	16.4 ± 2.3[N.S.]	53.4 ± 2.3[N.S.]	911.1 ± 189.9[a]
Pulmonary vein (N = 28)	26.4 ± 3.5[a]	44.7 ± 3.7[a]	340.2 ± 93.7[a]
Inferior vena cava (N = 14)	9.6 ± 4.2[a]	52.3 ± 8.1[N.S.]	740.4 ± 437.9[a]
Aorta (N = 14)	12.3 ± 3.7[a]	56.8 ± 12.1[N.S.]	2167.3 ± 484.2[a]

[a] $P < 0.0001$ compared to the mean parameter values in the lung parenchyma.
N.S. = Not significant.
SI = signal intensity, $\%T_{min}$ = (delay time after trigger R-wave showing the minimum SI/R-R wave interval) × 100, %Tmax = (delay time after trigger R-wave showing the maximum SI/R-R wave interval) × 100, ΔSI_{ECG} = (the maximum SI − background noise SI) − (the minimum SI − background noise SI).

within the proximal lumens of the bronchial trees surrounding the balloon-occluded site in 10 of these dogs (Fig. 2). The location and extent of the aerosol defects on the subtracted Gd-DTPA aerosol images appeared to nearly match those of the perfusion defects on the ECG-gated PW images in all 14 AO dogs (Fig. 2). After Gd-DTPA aerosol inhalation, the maximum supplemental SI increases in the unaffected lungs in the intravenous Gd-DTPA-enhanced PAPP images were 384% ± 97, and this enhancement was significantly greater than that of Gd-DTPA aerosol ($P < 0.0001$).

In these AO dogs, the intratracheal balloon had been adequately inserted at the target bronchi of these dogs on the x-ray fluoroscopy immediately after the MR study, without noticeable overinflation or volume loss in the obstructed lung areas.

PE Dogs

On the ECG-gated preparation scans of the 19 pulmonary embolic (PE) dogs, the SI of the embolized lung areas was persistently high throughout the cardiac cycle, although the SI loss during systole was apparent in nonembolized lung areas. The subtracted ECG-gated PW images visualized perfusion defects in the embolized areas, in consensus of the two observers (Figs. 4 and 5). There was a significant difference in the ΔSIECG between the embolized and nonembolized lungs areas (180.3 ± 40.2 vs. 48.4 ± 22.7; $P < 0.0001$). The subtracted intravenous Gd-DTPA-enhanced PAPP images also showed the perfusion defects. The location and extent of these perfusion defects were nearly consistent with those on the ECG-gated PW images (Figs. 4 and 5). The mean %ΔSIGd-DTPA of the embolized lung areas was significantly less than that of the nonembolized areas (113.7% ± 91.3 vs. 609.0% ± 128.3; $P < 0.0001$). However, after the pulmonary arterial phase images of the intravenous GD-DTPA-enhanced dynamic study, some enhancement of the affected areas was seen, probably due to the anastomotic/collateral perfusion. There was a significant linear correlation between the affected-to-unaffected lung %ΔSIGd-DTPA and ΔSIECG ratios ($r = 0.621$, $P < 0.005$), although the mean ΔSIECG ratio was significantly greater than the mean %ΔSIGd-DTPA ratio (0.27 ± 0.12 vs. 0.18 ± 0.13; $P < 0.01$) (Fig. 3B).

In the Gd-DTPA aerosol study, both the affected and unaffected areas showed fairly uniform Gd-DTPA aerosol deposition in 13 of these dogs, with relatively small embolized areas (Fig. 4). However, in the remaining 6 dogs, with widely embolized areas, Gd-DTPA aerosol deposition was decreased in the affected lung areas (Fig. 5). Overall, the mean maximum %ΔSIaerosol of the affected areas was significantly less than that of the unaffected areas (218.2% ± 68.8 vs. 249.9% ± 44.1; $P < 0.05$). After Gd-DTPA aerosol inhalation, the maximum supplemental SI increases in the unaffected lungs in the intravenous Gd-DTPA-enhanced PAPP images were 354% ± 87, and this enhancement was significantly greater than that of Gd-DTPA aerosol ($P < 0.0001$).

DISCUSSION

The present ECG-gated FSE MR sequence allowed the image acquisition of the cardiac-dependent pulsatile

Table 2
Signal Intensity on ECG-Gated FSE Perfusion MR Images in Normal Dog Lungs

	Right lung		Left lung	
	Ventral lung ($N = 14$)	Dorsal lung ($N = 14$)	Ventral lung ($N = 14$)	Dorsal lung ($N = 14$)
Diastole arbitrary maximum SI	357.8 ± 69.4	473.0 ± 124.6	392.0 ± 68.0	451.4 ± 123.2
	$P < 0.0001$	$P < 0.0001$	$P < 0.0001$	$P < 0.0001$
Systole arbitrary minimum SI	230.6 ± 80.3	246.4 ± 103.2	250.5 ± 79.5	226.1 ± 150.9
Δ SI_{ECG}	127.2 ± 30.3	226.6 ± 50.3	141.4 ± 35.2	225.2 ± 82.8
	$P < 0.0001$		$P < 0.005$	

SI = signal intensity, ΔSI_{ECG} = (the maximum SI − background noise SI) − (the minimum SI − background noise SI).

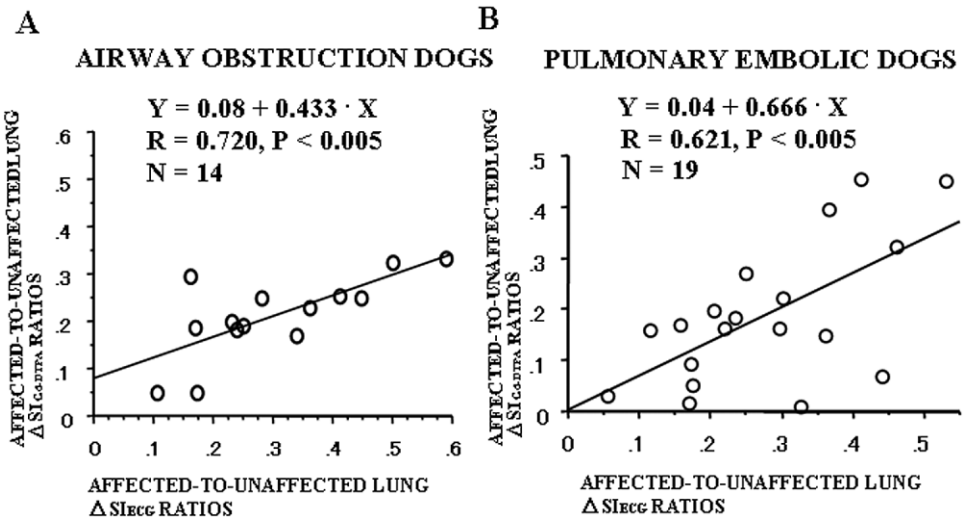

Figure 3. The comparison between the affected-to-unaffected lung %ΔSIGd-DTPA and ΔSIECG ratios in the 14 AO dogs (**A**) and 19 PE dogs (**B**). There was a significant linear correlation between the affected-to-unaffected lung %±SIGd-DTPA and ±SIECG ratios in both the AO dogs ($r = 0.720$, $P < 0.005$) and PE dogs ($r = 0.621$, $P < 0.005$). However, in these two models, the mean %ΔSIGd-DTPA ratio was significantly less than the mean ΔSIECG ratio (0.21 ± 0.08 vs. 0.30 ± 0.14; $P < 0.01$, and 0.27 ± 0.12 vs. 0.18 ± 0.13; $P < 0.01$, respectively).

lung parenchymal SI changes, and the subtracted noncontrast ECG-gated PW images between the systolic and diastolic phase images effectively visualized the perfusion defects in the affected lung areas in both the AO and PE animals. These perfusion defects were well consistent with those on the subtracted intravenous Gd-DTPA-enhanced PAPP images. The ECG-gated perfusion MR images allowed the subsequent Gd-DTPA aerosol MR study in the same dog, and these combined MR images effectively defined the matched or mismatched Gd-DTPA aerosol deposition and perfusion defects in the affected areas. Although the present results were preliminarily obtained only from the dog lower lungs, with some different anatomical and physiological characteristics from human lungs (11–13), this combination MR study may have potential ability for noninvasively defining regionally impaired lung function associated with AO and pulmonary embolism.

The present ECG-gated FSE sequence provided the images of cardiac-dependent pulsatile lung SI changes by minimizing magnetic susceptibility associated with the large air and tissue interface in the lungs (14–16). The SI changes during a cardiac cycle in the normal lungs may be caused by the blood flow velocity variations in the amount of dephasing and rephasing by magnetic field gradients. In a relatively fast flow, phase coherence generated with the 90° pulse in a multiecho sequence is not completely refocused for any subsequent echoes, resulting in substantial reduction in the SI (16,18–21). The signal loss during systole may result from a flow void effect due to the fast flow velocity in the vascular networks, and the recovered SI during diastole

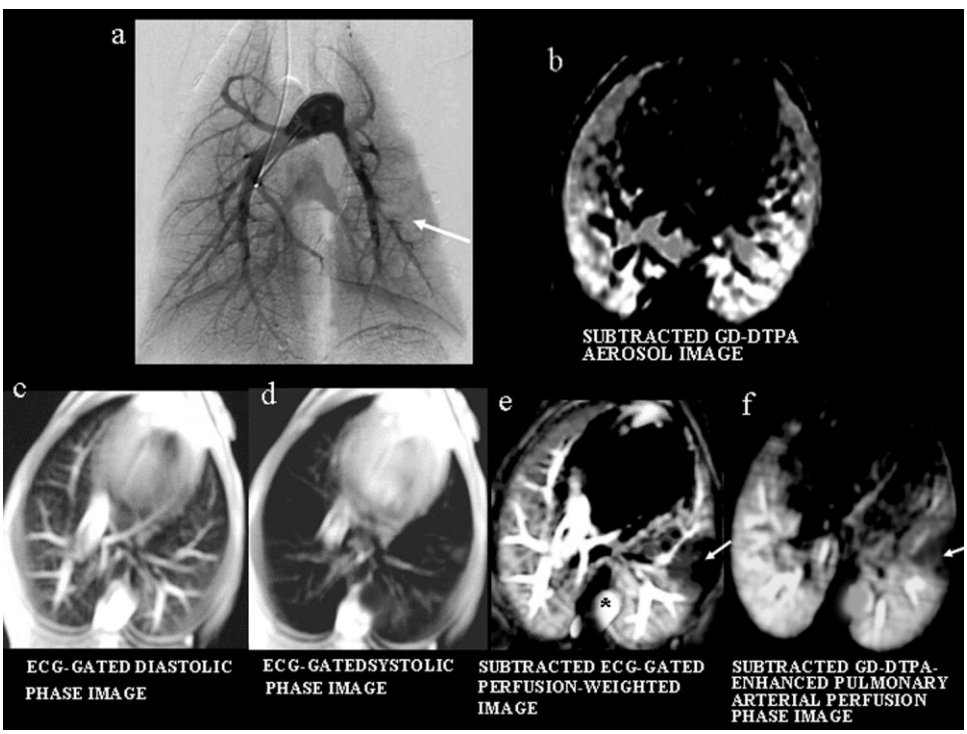

Figure 4. MR studies in a PE dog with a relatively small embolized lung area. Pulmonary arteriography (**a**) shows an embolization of the branch of the left lower pulmonary artery with enbucrilate (arrow). The subtracted Gd-DTPA aerosol MR image (**b**) shows fairly uniform aerosol deposition in both lungs. The subtracted ECG-gated PW image (**e**) derived from the diastolic and systolic phase images (TReff/TEeff = 919/80 msec) (**c** and **d**) shows a perfusion defect in the affected lung area (e, arrow), which nearly matches that on the subtracted intravenous Gd-DTPA-enhanced PAPP image (**f**, arrow). * = The round structure is the descending thoracic aorta (e).

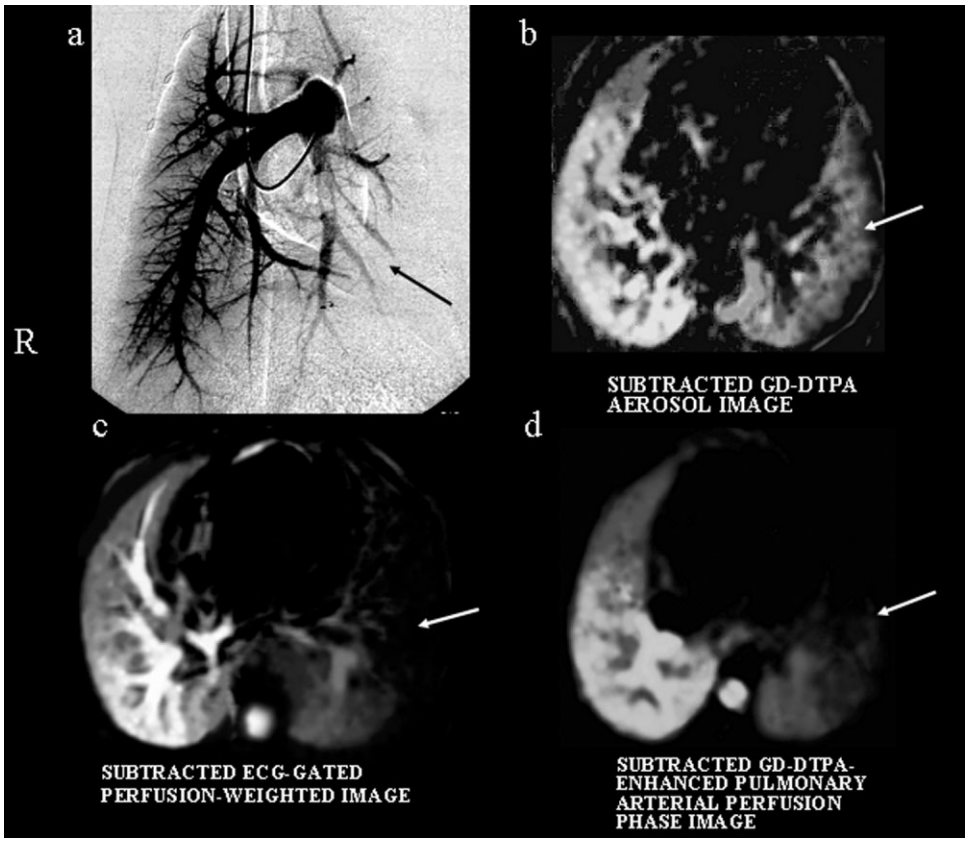

Figure 5. MR studies in a PE dog with a widely embolized lung area. Pulmonary arteriography (**a**) shows the extended embolization of the left lower pulmonary arteries (arrow). The subtracted Gd-DTPA aerosol MR image (**b**) shows decreased aerosol deposition in the left embolized lung area (arrow). The subtracted ECG-gated PW image (TReff/TEeff = 782/80 msec) shows a perfusion defect in the embolized lung (**c**, arrow), which almost matches that on the subtracted intravenous Gd-DTPA-enhanced PAPP image (**d**, arrow).

may result from the slow flow velocity (16,21). This is suggested by the results of our previous flow phantom study using a water stream with variable flow velocities ranging from 0–56 cm/second and the same FSE sequence used for the present multiphase ECG-gated MRI, where a linearity between the SI loss of the water stream and flow velocity was found in the flow velocity, ranging from 7.2–57 cm/second (16). The greatest ΔSIECG of the aorta and the lowest ΔSIECG of the lung parenchyma can be explained by these flow effects, although the lowest lung parenchymal ΔSIECG may be partly caused by the susceptibility effect of the lung tissues. The lung SI changes during cardiac cycles may be mainly due to the pulmonary arterial blood flow, since approximately 95% of pulmonary circulation is normally supplied from the pulmonary artery (11,12,21). In fact, Tmin and Tmax, representative of the arrival time to the greatest SI loss and recovery in the lungs, were synchronized with those of the pulmonary artery. The pulmonary artery shows a peak inflow at the middle phase of the cardiac systole, which may correspond to the lung signal loss during systole (18,19,21). The pulmonary veins show moderate speed flow during the ventricular contraction period, but they show a short, slow-flow phase before the atrial contraction period, which may correspond to the high lung parenchymal SI during diastole (24,25). The greater SI in the normal dependent lungs can be explained by the gravity effects on pulmonary perfusion (greater blood flow velocity), although the greater blood volume in these lungs also may partly contribute to this greater SI (2,4,18,19,26–28). Our previous flow phantom study showed that the linearity between the SI loss of water stream and flow velocity was lost in the relatively low flow velocity of less than 4.3 cm/second, with almost steady SI (16). Therefore, the lung SI difference between systole and diastole might reflect only the greater blood flow velocity change in the relatively large vascular networks, since blood flow in the alveolar microvasculatures is constantly slow, less than approximately 0.3–0.5 mm/second (20,27–29). However, the present study showed a significant linear correlation between the affected-to-unaffected lung %ΔSIGd-DTPA and ΔSIECG ratios in the lung parenchyma of the living animals. The ECG-gated PW images can partly reflect the relatively low blood flow fraction in the lung parenchyma in the living animal. Further comparison with perfusion scintigrams and/or pulmonary angiography is warranted in this issue.

The present subtracted ECG-gated PW MR images effectively visualized the perfusion defects in the airway-obstructed lung areas. Regional hypoxemia in the hypoventilated lungs is considered to attribute to these perfusion defects. Regional hypoxemia has a direct action on the smooth muscle of pulmonary arteries and partly on the small pulmonary veins, and elicits hypoxic vasoconstriction leading to regional hypoperfusion (29–35). These ECG-gated perfusion images also effectively visualized the perfusion defects in the embolized lung areas. However, both in the airway-obstructed and embolized areas, the perfusion defect clarity against the unaffected lungs was lower on the ECG-gated perfusion images than on the intravenous Gd-DTPA-enhanced PAPP images. It may be caused by the effect of signal

averaging of the ECG-gated image acquisition, and may be partly caused by the flow void effects associated with the compensatory anastomotic/collateral perfusion in the affected areas. As seen on the post-PAPP images of the intravenous Gd-DTPA-enhanced dynamic studies in the present animals, and as shown in previous studies, some anastomotic/collateral perfusion may be present in the affected areas (9,12,13).

As frequently seen in the AO dogs, the central Gd-DTPA aerosol hyperdeposition with defects in the distal air space may be indicative of the presence of AO. Gd-DTPA aerosol deposition to the obstructed wall should be accelerated due to turbulent bronchial airflow in the balloon-occluded bronchi (36–38). The decreases of Gd-DTPA aerosol deposition in the widely embolized lung areas in the present PE dogs may be partly caused by transient regional bronchial spasms and lung stiffening after acute pulmonary embolism (39,40). Besides, Gd-DTPA aerosol may be preferentially diverted to nonembolized lung zones, resulting in a temporal local deposition defect in the widely embolized areas (40).

The present ECG-gated perfusion MR image has the advantages of superior anatomic resolution, compared with perfusion scintigrams, and no use of contrast materials, which allows a simultaneous Gd-DTPA aerosol MR study. The Gd-DTPA aerosol MR image has the advantages of wide availability and low cost, and no requirement of modification of MR hardware. As shown in the present preliminary study, these combination MR studies may have potential ability for noninvasively defining regionally impaired lung function in AO and pulmonary embolism. However, the drawbacks of these images include the subtraction process being sensitive to misregistration due to bulk motion. The use of a respiration navigator gating or normalized subtraction technique may partly improve this artifact. The slice thickness of 20 mm of the present ECG-gated perfusion MR image should be reduced to detect a small/ill-defined perfusion defect. This perfusion image may be insensitive to very slow flow velocity, as indicated by our previous water flow phantom study, and the lowest blood flow limit in the peripheral vascular networks of the lungs detectable with these images is unknown. This image may have difficulty in obtaining a high-quality image in extreme cases with very low cardiac output and may fail to detect a perfusion defect in the affected lung areas. Temporal global changes in cardiac output may alter the affected-to-unaffected lung contrast and may interrupt accurate interstudy comparison in individual subjects. The ability of the combination MR studies to detect smaller regions of lung function impairment is also not clarified. Further studies are warranted in these issues, and comparisons with perfusion scintigrams and/or pulmonary angiography in various lung diseases are also needed to evaluate whether the present ECG-gated image can be called pulmonary perfusion image in the traditional sense.

REFERENCES

1. Chen Q, Levin DL, Kim D, David V, McNicholas M, Chen V. Pulmonary disorders: ventilation-perfusion MR imaging with animal models. Radiology 1999;213:871–879.
2. Cremiillieux Y, Berthezene Y, Humblot H, et al. A combined ^{1}H perfusion/^{3}He ventilation NMR study in rat lungs. Magn Reson Med 1999;41:645–648.
3. Viallon M, Berthezene Y, Decorps M, et al. Laser-polarized ^{3}He as a probe for dynamic regional measurements of lung perfusion and ventilation using magnetic resonance imaging. Magn Reson Med 2000;44:1–4.
4. Berthezene Y, Vexler V, Clement O. Contrast-enhanced MR imaging of the lung: assessments of ventilation and perfusion. Radiology 1992;183:667–672.
5. Schreiber WG, Markstaller K, Weiler N, et al. Breathhold ^{19}F-magnetic resonance imaging of lung ventilation using SF6 gas. Fortschr Rontgenstr 2000;172:500–503.
6. Amundsen T, Kvaerness J, Jones RA, et al. Pulmonary embolism: detection with MR perfusion imaging of lung. A feasibility study. Radiology 1997;203:181–185.
7. Montogomery AB, Paajanen H, Brasch RC, Murray JF. Aerosolized gadolinium DTPA enhances the magnetic resonance signal of extravascular lung water. Invest Radiol 1987;22:377–381.
8. Misselwitz B, Muhler A, Heinzelmann I, Bock JC, Weinmann HJ. Magnetic resonance imaging of pulmonary ventilation. Initial experiences with a gadolinium-DTPA-based aerosol. Invest Radiol 1997; 32:797–801.
9. Haage P, Adam G, Karaagac S, Pfeffer J, et al. Mechanical delivery of aerosolized gadolinium-DTPA for pulmonary ventilation assessment in MR imaging. Invest Radiol 2001;36:240–243.
10. Amundsen T, Kvaerness J, Aadahl P, et al. A closed-chest pulmonary artery occlusion/reperfusion model in the pig. Detection of experimental pulmonary embolism with MR angiography and perfusion MR imaging. Invest Radiol 2000;35:295–303.
11. Suga K, Ogasawara N, Matsunaga N, Sasai K. Perfusion characteristics of oleic acid-injured canine lung on Gd-DTPA-enhanced dynamic magnetic resonance imaging. Invest Radiol 2001;36:386–400.
12. Suga K, Mikawa M, Ogasawara N, Okazaki H, Matsunaga N. Potential of (Gd-DTPA-Mannan)-coated liposome particles as a contrast agent for pulmonary perfusion magnetic resonance imaging: an initial animal study. Invest Radiol 2001;36:136–145.
13. Suga K, Ogasawara N, Okada M, Matsunaga N, Arai M. Regional lung functional impairment in acute airway obstruction and pulmonary embolic dog models assessed with gadolinium-based aerosol ventilation and perfusion magnetic resonance imaging. Invest Radiol 2002;37:281–291.
14. Haage P, Karaagac S, Adam G, Spuntrup E, Pfeffer J, Gunther RW. Gadolinuim containing agents for pulmonary ventilation magnetic resonance imaging: preliminary results. Invest Radiol 2002;37: 120–125.
15. Ogasawara N, Suga K, Ito K, et al. Demonstration of perfusion defect for pulmonary embolism in a canine model: feasibility of ECG-gated 2D half-Fourier FSE. In: Proceedings of the 9th Annual Meeting of ISMRM, Glasgow, Scotland 2001. 9:1995.
16. Suga K, Ogasawara N, Munemasa O, et al. Potential of noncontrast electrocardiogram-gated half-Fourier fast-spin-echo magnetic resonance imaging to monitor dynamically altered perfusion in regional lung. Invest Radiol 2002;37:615–625.
17. Suga K, Ogasawara N, Tsukuda T, Matsunaga N. Assessment of regional lung ventilation in dog lungs with Gd-DTPA aerosol ventilation MR imaging. Acta Radiol 2002;43:282–291.
18. Miyazaki M, Ichinose N, Sugiura S, Kasai V, Kanazawa H, Machida Y. A novel MR angiography technique: SPEED acquisition using half-Fourier RARE. J Magn Reson Imaging 1998;8:505–507.
19. Miyazaki M, Sugiura S, Tateishi F, Wada F, Kasai Y, Abe H. Noncontrast-enhanced MR angiography using 3D ECG-synchronized half-Fourier fast spin echo. J Magn Reson Imaging 2000;12:776–783.
20. Kawakami S, Nakamura K, Miyazaki M, et al. ECG-gated MR imaging of the lung parenchyma using 2D short-echo-spacing half-Fourier FSE. In: Proceedings of the 9th Annual Meeting of ISMRM, Denver, 2000. 8:299.
21. Keilholz-George S, Lange EE, Knight-Scott J. Exploiting the cardiac-dependent signal intensity in the lung for MR pulmonary imaging. In: Proceedings of the 9th Annual Meeting of ISMRM, Glasgow, 2001. 9:1993.
22. Suga K, Yuan, Y, Ogasawara N, Tsukuda T, Matsunaga N. Altered clearance of gadolinium-DTPA aerosol from bleomycin-injured dog lungs: initial observations. Am J Respir Crit Care Med 2003;165: 1704–1710.

23. National Research Council. Guide for the care and use of laboratory animals, 7th edition. Washington, DC: National Academy Press; 1996.
24. Shandas R, Weinberg C, Ivy DD, et al. Development of a noninvasive ultrasound color M-mode means of estimating pulmonary vascular resistance in pediatric pulmonary hypertension: mathematical analysis, in vitro validation, and preliminary clinical studies. Circulation 2001;104:908–913.
25. Morkin E, Collins JA, Goldman HS, Fishman AP. Pattern of blood flow in the pulmonary veins of the dogs. J Appl Physiol 1965;20: 1118–1128.
26. West JB. Structure and function. In: West JB, editor. Respiratory physiology—the essentials, 5th edition. Baltimore: Wilkins & Wilkins; 1995. p 1–10.
27. West JB, Dollery CT, Naimark A. Distribution of blood flow in isolated lung: relation to vascular and alveolar pressure. J Appl Physiol 1964;19:713–724.
28. MacNee W, Martin BA, Wiggs BR, Belzberg AS, Hogg JC. Regional pulmonary transit times in humans. J Appl Physiol 1989;66:844–850.
29. Isawa T, Wasserman K, Taplin GV. Lung scintigraphy and pulmonary function studies in obstructive airway disease. Am Rev Respir Dis 1970;102:161–172.
30. Suga K, Nishigauchi K, Kume N, Uchisako H, Yoshimizu T, Nakanishi T. Delayed restoration of lung perfusion after removal of aspirated foreign body. Clin Nucl Med 1995;20:1032–1033.
31. Clercx C, van den Brom WE, Stokhof AA, de Vies HW. Pulmonary scintigraphy in canine lobar and sublobar airway obstruction. Lung 1989;167:213–224.
32. Morrell NW, Nijran KS, Biggs T, Seed WA. Changes in regional pulmonary blood flow during lobar bronchial occlusion in man. Lung 1994;86:639–644.
33. Isawa T, Wasserman K, Taplin GV. Lung scintigraphy and pulmonary function studies in obstructive airway disease. Am Rev Respir Dis 1970;102:161–172.
34. West JB. Environmental and other diseases. In: Coryell PA, editor. Pulmonary pathophysiology—the essentials, 4th edition. Baltimore: Williams & Wilkins; 1992. p 129–147.
35. West JB. Mechanics of breathing. In: Satterfield TS, editor. Respiratory physiology—the essentials, 5th edition. Baltimore: Williams & Wilkins; 1995. p 89–116.
36. Rizk NW, Luce JM, Hoeffel JM, Price DC, Murray JF. Site of deposition and factor affecting clearance of aerosolized solute from canine lung. J Appl Physiol 1984;56:723–729.
37. O'Riordan TG, Walser L, Smaldone GC. Changing patterns of aerosol deposition during methacholine bronchoprovocation. Chest 1993;103:1385–1389.
38. Chung SK, Kim HH, Bank VW. Prestenotic bronchial radioaerosol deposition: a new ventilation scan sign of bronchial obstruction. J Nucl Med 1997;38:71–74.
39. Mori Y, Alderson PO, Berman L. Effect of acute experimental pulmonary arterial occlusion on the deposition and clearance of technetium-99m-DTPA radioaerosols. J Nucl Med 1994;35:1351–1357.
40. Isawa T, Taplin G, Beazell J, Criley M. Experimental unilateral pulmonary artery occlusion. Acute and chronic effects on relative inhalation and perfusion. Radiology 1972;102;101–109.